Journal of Power Sources 267 (2014) 784–792

Contents lists available at ScienceDirect

Journal of Power Sources

journal homepage: www.elsevier.com/locate/jpowsour

Simulative method for determining the optimal operating conditions for a cooling plate for lithium-ion battery cell modules

Joshua Smith [a, b, *], Michael Hinterberger [b], Peter Hable [b], Juergen Koehler [a]

[a] Institut für Thermodynamik (IfT), Technische Universität Braunschweig, Hans-Sommer-Str. 5, 38106 Braunschweig, Germany
[b] AUDI AG, 85045 Ingolstadt, Germany

HIGHLIGHTS

- A method to optimize operating conditions for multiple objectives is presented.
- The method is demonstrated on a cooling plate for an electric vehicle battery.
- The method can be generalized to any battery thermal management system.
- The appropriate simulation model for the analyzed case is discussed.
- The results enhance the effectiveness of dynamic one-dimensional simulations.

ARTICLE INFO

Article history:
Received 17 February 2014
Received in revised form
26 May 2014
Accepted 1 June 2014
Available online 10 June 2014

Keywords:
Lithium-ion
CFD
Thermal management
Electric vehicle
Cooling plate

ABSTRACT

Extended battery system lifetime and reduced costs are essential to the success of electric vehicles. An effective thermal management strategy is one method of enhancing system lifetime increasing vehicle range. Vehicle-typical space restrictions favor the minimization of battery thermal management system (BTMS) size and weight, making their production and subsequent vehicle integration extremely difficult and complex. Due to these space requirements, a cooling plate as part of a water–glycerol cooling circuit is commonly implemented.

This paper presents a computational fluid dynamics (CFD) model and multi-objective analysis technique for determining the thermal effect of coolant flow rate and inlet temperature in a cooling plate—at a range of vehicle operating conditions—on a battery system, thereby providing a dynamic input for one-dimensional models. Traditionally, one-dimensional vehicular thermal management system models assume a static heat input from components such as a battery system: as a result, the components are designed for a set coolant input (flow rate and inlet temperature). Such a design method is insufficient for dynamic thermal management models and control strategies, thereby compromising system efficiency. The presented approach allows for optimal BMTS design and integration in the vehicular coolant circuit.

1. Background and motivation

Electric vehicles rely on high capacity and energy density power storage systems to extend the vehicle range and mass-market appeal. Currently, automobile manufacturers implement various Lithium-ion battery cells because they offer high power densities and are commercially available. The cells are high in cost [1] making a maximization of their lifetime desirable, which differentiates them from consumer cells found in small electronics such as laptops. Lithium-ion cells age not only over time, but also due to other influences including their state of charge (SOC), charging or discharging rate (C-rate), the depth of discharge (DOD), and extreme temperatures [2]. All these factors have varied effects on the multitude of cell chemistries in use today, but it is clear that temperature has a universal influence on the performance degradation of nearly all positive electrode and electrolyte chemistries [3]. High-current cycling, which is required for high performance and rapid-charging applications, significantly increases the temperature in the cell [1]. According to Bandhauer et al. [3] heat produced in a cell stems from three fundamental sources: activation interfacial kinetics, concentration species transport, and ohmic Joule heating

* Corresponding author. AUDI AG, 85045 Ingolstadt, Germany. Tel.: +49 841 89 760756.
E-mail address: joshua.smith@audi.de (J. Smith).

http://dx.doi.org/10.1016/j.jpowsour.2014.06.001
0378-7753/

from the movement of charged particles losses, which becomes very significant for larger cell sizes such as those discussed in this paper. The goal of a BTMS is to increase the lifetime of Lithium-ion cells by regulating the temperature influences on the cell. A BTMS is especially effective when cells are susceptible to high rates of charging (e.g. rapid charging or regenerative breaking) and discharging (e.g. high performance vehicles, plug-in hybrids) and when the vehicle is operated in very high or low ambient temperatures.

Maintaining temperatures between approximately 25 and 35 °C while achieving a uniform temperature across each cell and across cell packs (so called modules) helps limit aging [4]. Pesaran et al. [4] have shown on the example of a pouch cell that large temperature gradients over a single cell reduces its lifetime. Premature aging of a single cell degrades the performance of a module noticeably because of the circuitry between the cells: when connected in series, the weakest cell will influence the maximum capacity of the system.

Thermal management itself is not the primary challenge, but rather the extremely restricted space available to a BTMS in a modern vehicle. All battery system components including the BTMS must vie for space with the multitude of components in a modern luxury vehicle. Since millimeter increases in the dimensions of the BTMS cannot be tolerated, it is critical to optimize the potential of the BTMS while minimizing the occupied area.

In the case of an active thermal management system, the ideal working fluid is already present in the vehicle (e.g. air, antifreeze or refrigerant) and available within the desired temperature range. The amount of additional components required for the BMTS are thereby reduced, effectively lowering the size, weight, and ultimately the cost of the system. For example many production hybrid-electric vehicles (HEV) use forced air for cooling and heating, taking advantage of existing technologies within the vehicle; however, battery systems in plug-in hybrid vehicles (PHEV) often have greater thermal management requirements because they operate under high charge and discharge rates.

In the case of a PHEV liquid cooling is advantageous, especially considering that the system is generally integrated into a vehicle with an internal combustion engine, leaving even less space for the BTMS [5]. Some sort of cooling plate is implemented in most currently available plug-in hybrid electric (PHEV) vehicles and mentioned in numerous patents from major vehicle and cooling system manufacturers [6–10] and is therefore the focus of this paper. Cooling from the small surface at the bottom of a prismatic cell is thermodynamically suboptimal; however, there are numerous other factors that have made cooling plates prominent such as the minimal space requirements in the vehicle, the availability of components from predominant cooling system manufactures, and the ability of the cooling plate to provide structural support to the battery and integrate into a so-called battery module (see Section 4).

The quantities of interest for evaluating the performance of the cooling plate are the (1) temperature differences over individual cells, (2) amongst the cells (i.e. within a module), (3) the maximum cell temperature, and the (4) coolant pressure loss through the plate. The maximum temperature and temperature difference over an individual cell must be minimized in order to slow aging of the cell; the temperature differences over individual cells in a module must be similar in order to avoid inhomogeneous aging amongst the cells and subsequent capacity reduction due to the failure of a single cell electrically connected in series with others. The maximum temperature must also be controlled to ensure safe operation. The pressure loss influence the pump size required, which influences energy consumption and vehicle integration by requiring mechanically stronger cooling plates to withstand the higher pressure forces, leading to higher costs. These costs must be justified by an improvement in the performance of the cooling plate resulting in an increased cell-lifetime.

This paper presents a simulative method using commercially available computational fluid dynamics (CFD) software to predict the optimal cooling circuit operating conditions (coolant volumetric flow rate and inlet temperature) for a variety of vehicle operating conditions (ambient temperature, vehicle speed and SOC) in order to minimize the pressure loss across the BTMS, the temperature gradients over and amongst the cells, and the maximum cells temperatures. The analysis is performed on a battery module developed in the research project *eProduction* (presented in Section 2.3). Various simulative models for the module are first compared in order to find the most efficient yet accurate cell model.

The goal of this method is to provide BTMS designers with universal results (i.e. not flow channel geometry specific) to assist in designing cooling systems economically for optimal vehicle integration while extending cell life-time and vehicle range. These results also extend the effectiveness of vehicular one-dimensional thermal management system models because the thermal state of the battery is calculated over the complete range of coolant flow rates and inlet temperatures, making dynamic feedback control possible and greatly enhancing the efficiency of the vehicle's thermal management system.

2. Design considerations for battery modules and a CFD-Model

2.1. Energy consumption of the BTMS

Currently available electric vehicles from the Tesla Model S to the Nissan Leaf consume approximately 0.187 kWh km^{-1} according to the manufacturer's specifications. Based on this data, the effect of pump size alone on vehicle range at different average speeds is calculated and shown in Table 1.

Losses to cooling system pumps clearly become more significant at lower speeds, when the electric motor consumes less power, yet the pump remains on. Table 1 further illustrates the benefit of dynamic thermal system control, as the total pump power is most likely not required continuously. The simulative method presented in this paper identifies the required pump power at various operating points, providing the necessary input for a one-dimensional vehicle thermal system model.

2.2. The cell: heat source for the CFD model

This analysis considers the prismatic SANYO/PANASONIC PHEV-2, 25 Ah Lithium-ion cell, which was developed for the

Table 1
Energy consumption of coolant circuit pump as percent of total energy consumption at various vehicle speeds.

Vehicle average speed (km h^{-1})	% of total energy consumption 50 W pump	% of total energy consumption 100 W pump
10	2.7%	5.3%
20	1.3%	2.7%
30	0.9%	1.8%
40	0.7%	1.3%
50	0.5%	1.1%
60	0.4%	0.9%
70	0.4%	0.8%
80	0.3%	0.7%
90	0.3%	0.6%
100	0.3%	0.5%

automotive plug-in hybrids. Cell chemistry and the mechanisms for cell heat loss are not the focus of this analysis, but rather the influence of the BTMS on the thermal characteristics the cell. A simplified diagram of a prismatic cell is shown in Fig. 1. The electrochemical construction of the prismatic cell is essentially similar to a cylindrical cell, except that it is compressed into an oval "jelly roll" and inserted into an aluminum cell. The anode and cathode are then bundled to copper and aluminum tabs on either side of the jelly roll and connected to the cell terminals at the top of the cell.

The primary source of cell heat loss is internal electrical resistance. The internal resistance varies primarily as a function of electrical current, SOC, external temperature, and state of health (SOH). Values of internal resistances presented in the manufacturer's data sheet are used as a guideline to determine a range of feasible cell heat loss values occurring at various vehicle speeds in various ambient conditions with battery cells at various SOC and SOH. Additional thermal properties of the cell are also taken from the manufacturer's data sheet; from these thermal properties the cell can be modeled as a uniform heat source because—as shown by the relatively small Biot (Bi) Number ($Bi < 0.1$)—the conduction within the cell is significantly more dominant than the convection from the cell to still air.

It should be noted that many studies exist showing the benefit of considering a cell as a non-uniform heat source, but such research has been conducted on other cell types such as pouch cells [11], which appear more likely to show temperature gradients than PHEV-2 cells. This may be due to the thicker cell casing of the PHEV-2 cell, through which the rate of conduction is five to ten times slower than through the pouch cell casing. Thus, during the dynamic operation of the cell, the temperature gradients do not have time to develop on the cell surface. Additionally, the anode and cathode tabs are on opposite sides of the jelly roll, which Pesaran et al. and Teng et al. have shown to reduce temperature gradients in comparison to pouch cell-typical layouts that group the tabs on a single side of the cell [4,12].

The true limit to battery system performance is the premature aging of an individual cell; however, it is more practical to design a cooling system layout to thermally control all cells equally from the beginning of their lifetime. The implementation of a cell model as a heat source instead of a surface heat flux boundary condition at the surface of the cooling plate is advantageous because of the anisotropic conduction in the cell and because temperatures throughout the cross section of the cell can be calculated.

2.3. The cell-module: building block

A commonly implemented building block in the realization of a battery system is a cell-module. The modular design allows for available space in various vehicles to be filled with "standard" modules consisting of a set number of cells to create the battery system. As such only one building block must be developed, reducing part and production costs due to the economy of scale. This analysis, though performed considering an eight cell module from the research project *eProduction*, is universally applicable to other BTMS concepts. In the case of prismatic cells, the module entails electrical contacts via bus bars at the cell terminals, electrical insulation of the cell casings from one another (to prevent accidental short circuiting), and a compression member to withstand the expansion forces generated by the cells (upwards of 11 kN), as shown in Fig. 2.

A module can also have an autonomous battery management and control system (not shown in figure). The module must then be coupled to the BTMS to optimize the thermal contact but not jeopardize the electrical insulation between cells (if the cooling plate is electrically conductive). This is challenging because as for any manufactured product, dimensional tolerances exist among PHEV-2 cells. The result, pertaining to cooling plates, is a variation in the cell height. Aligning the bottom of all cell casings in the plane of the cooling plate provides the optimal contact, but the cell height tolerances are then displaced to the cell terminal. The current rigid cell bus-bars release large amounts of heat when incompletely contacted at the cell terminal [13], forcing the cooling plate to compensate the cell height tolerances. Various solutions to overcome the tolerances include:

- Selecting cells with similar heights
- Leaving air pockets and accept inhomogeneous contact area
- Filling potential air pockets with a material more conductive than air
- Pressing the cells to the cooling plate with high forces to enhance the contact through deformation of the cooling plate and electrically insulation elements.

Sorting through cells, however automated, is an expensive step from a production-oriented viewpoint as this process involves additional machinery, labor and time, and can never truly bring the tolerance to zero. Leaving air pockets creates additional thermally insulating layers and results in local hotspots, thereby increasing the temperature gradient across the module and causing

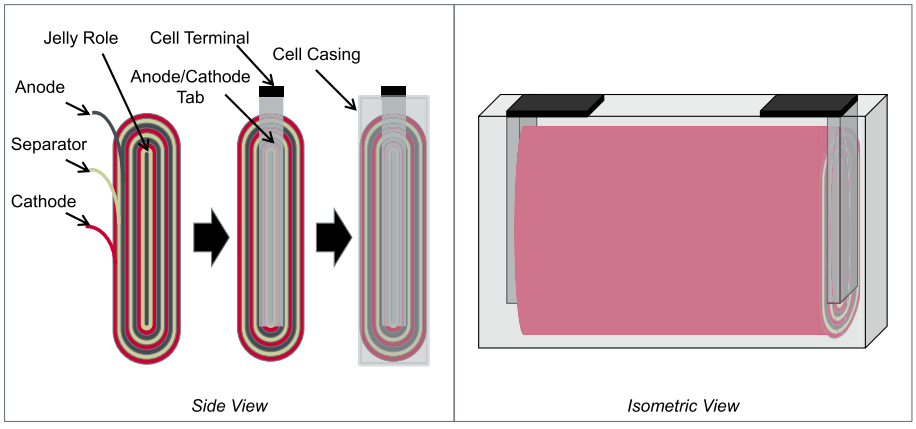

Fig. 1. Simplified schematic layout of a PHEV-2 prismatic cell.

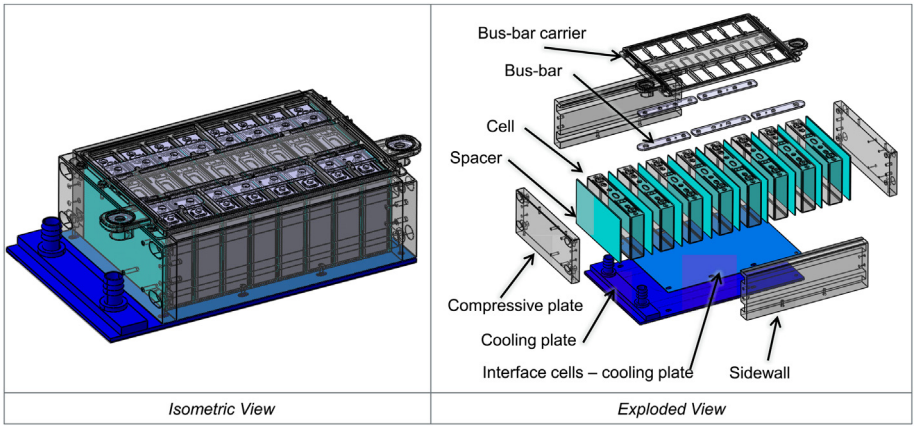

Fig. 2. Conceptual layout of a battery module for prismatic cells.

inhomogeneous cell aging. Filling the potential gaps with a thermally conductive material enhances the conductivity to the plate, but it must not undermine the electrical insulation between the cells. A ductile solid material such as a mat can fill air gaps, but its thickness should be minimized and thermal conductivity maximized. In some cases the module can be compressed to the cooling plate, allowing a ductile material to "fill" potential air pockets between cell casing and cooling plate. Applying force is an effective way to enhance the contact surface [10,14,15] because especially ductile materials will deform around the cell casing and required electrical insulation.

The necessary consideration of electrical insulation, thermal contact and expansion forces combined with the strict volumetric constraints imposed by a modern vehicle have combined to make cooling plates the state of the art in most patents and commercially available PHEVs using prismatic cells due to the complexity of applying potentially more effective cooling concepts. Realizing active cooling elements between cells, as is often the case with pouch cells [11,12,16,17], is more complex for prismatic PHEV-2 cells mostly due to the larger expansion forces of the cells. The aforementioned challenges drive up the cost and complexity for the production of the cooling plates and complete battery systems.

3. Model setup

Four CFD-models are compared to determine the most accurate yet computationally efficient representation of an *eProduction* module with a cooling plate. This model serves as the basis for the presented analysis method to determine the optimal coolant inlet temperature and flow rate at a variety of vehicle operating conditions. Commercially available CFD-software is used for the model generation, meshing, and solving. The model setup is critical to the effectiveness of the multi-objective optimization and analysis; therefore, the primary additional considerations—as well as the general process steps followed—are shown in Fig. 3 and are described in detail in the following sections.

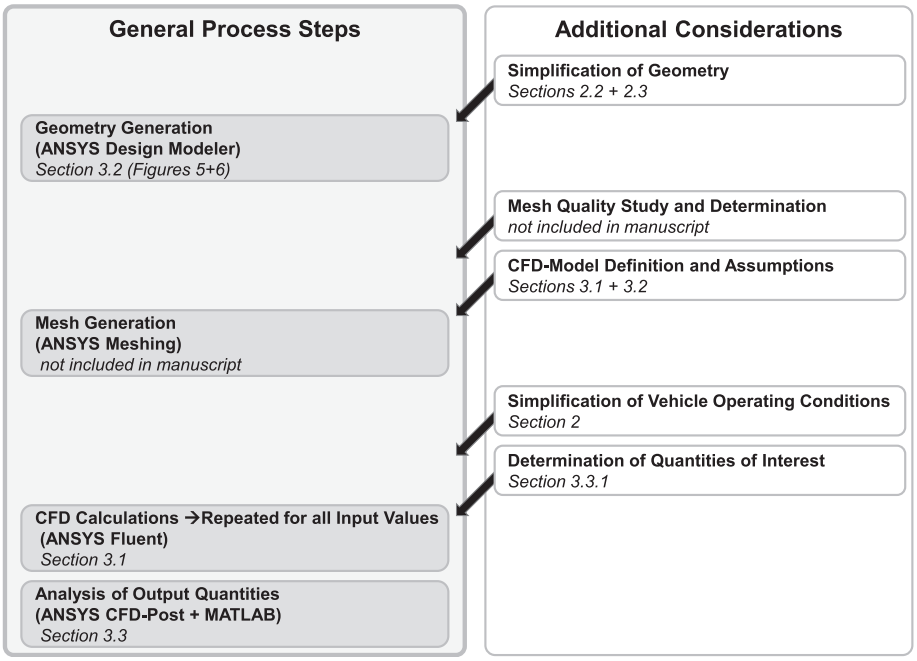

Fig. 3. General process steps and additional considerations for the simulation model and the multi-objective analysis method presented in the following sections. The text position of the detailed description is listed in italics under each heading.

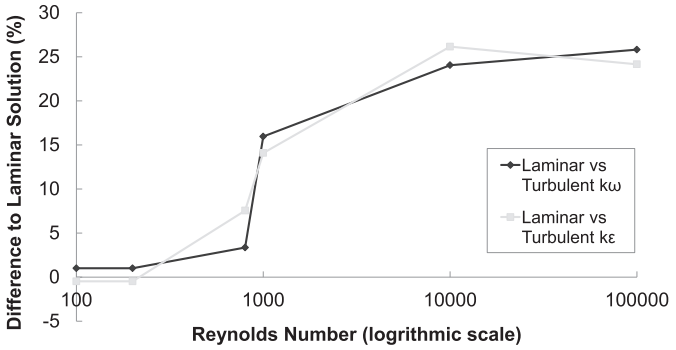

Fig. 4. Percentage difference of the calculated velocity along the centerline of the cooling plate channel for various turbulence models in comparison to the laminar solution as a function of Reynolds number (logarithmic scale).

3.1. General simulation environment and assumptions

Mass flow rates of the coolant antifrogen N mixed 50/50 with water [18] are calculated for a range of volumetric flow rates as a function of temperature; the mass flow rate and inlet temperature are the inlet boundary conditions in ANSYS Fluent. The density, specific heat capacity, and thermal conductivity of the cooling fluid are assumed constant, as they vary by approximately 1% over the examined temperature range; viscosity, however, varies significantly (≈47%) and is therefore described as a polynomial function in Fluent. A pressure outlet boundary condition is applied. A Fluent source term represents the heat loss of the actual cell at a various driving conditions, cell SOCs and ambient temperatures. All external walls are assumed adiabatic. The steady state solution is calculated with the Fluent CFD from an initial module temperature of 300 K. In the two-dimensional flow channel, the channel height is assumed to be the characteristic length. With this assumption, the flow is in the laminar and transition regions (Reynolds Number $< 10^5$) for the majority of cases; however, in order to assure uniform treatment with "extreme" cases in the transition region, all design points are calculated using the *k*–omega turbulence model. To ensure the validity of this decision, the discrepancies of the laminar, the realizable *k*–epsilon solution, and the SST *k*–omega solutions are compared over a variety of Reynolds Numbers at the centerline between two parallel plates.

As shown in Fig. 4, the discrepancies between the laminar and turbulent models are insignificant at low Reynolds Numbers, making the use of a turbulence model acceptable for this geometry. The SST *k*–omega turbulence model is applied because of its strength near solid walls over other traditional models [19]. The solution is obtained using the "coupled" method, the pseudo transient option, and the default timescale factor of 1. Solutions are iterated until the default FLUENT convergence criteria is reached. To obtain data regarding the temperature differences within and among cells as well as the pressure loss over the channel, expressions are created in CFD-Post and then applied as FLUENT output parameters (Table 2). The analysis method is presented in more detail in Section 3.3.

3.2. Simulative cell module model comparison

Using the model assumptions stated above, four types of models of the cell module are compared (see Fig. 5). The goal is to determine the cell module model that provides the most detail regarding the thermal behavior of the cells, yet is as computationally efficient as possible.

The four model types considered are:

- Two-dimensional "block" model
- Three-dimensional "block" model
- Two-dimensional "individual cell" model
- Three-dimensional "individual cell" model

The block models consider all eight cells of the module as a single component with uniform heat generation having the size and thermal properties of eight cells. The individual cell models consider the each cell as a uniform heat source, separated from other cells by a commercially available electrically insulating mat with relatively good thermal conductivity (compared to plastic). The cells are thermally coupled to the cooling plate via a commercially available, 1 mm thick ductile mat with relatively good thermal conductivity. For the purpose of the CFD-Analysis, a homogenous contact surface (i.e. no air pockets, constant thickness) is assumed. These materials are chosen in line with the goals of the research project *eProduction* (cost effectiveness, producibility). The BTMS height is also limited: the top plate, the fluid channel height, and the bottom plate ($h_{\text{contact plate}} + h_{\text{fluid}} + h_{\text{bottom plate}}$) total height is limited to 5 mm. Fig. 6 shows the conceptual composition of the cooling plate used in the CFD-model.

The cell module models are compared based on the values of the temperature difference over the module and maximum temperature values. The implementation of a the most simple—yet accurate—possible model is desired in order to save computational time and increase the amount of operational design points that can be compared. Because of the (current) lack of experimental validation, the most conservative model is preferred. General trends appearing across the model types are shown in Fig. 7.

As Fig. 7 shows, the maximum temperatures and temperature differences are generally higher for the individual cell models as compared to the block models and the two-dimensional models as

Table 2
Description of input parameter and quantities of interest.

Parameter	Description	Definition	Range
$\dot{\boldsymbol{Q}}$	Cell heat loss	Reflects the heat loss of the cell due to various charging and discharging conditions caused by various driving styles at various ambient temperatures and battery system SOCs.	5–40 W/Cell
T_{in}	Coolant inlet temperature	Temperature of the coolant at the inlet of the cooling plate.	0–40 °C
$\dot{\boldsymbol{V}}$	Coolant volumetric flow rate	Flow rate of the coolant entering the cooling plate. Converted to a mass flow rate for Fluent.	5–60 L min^{-1}
Δp	Pressure drop along cooling plate	Difference of the average pressure across inlet and the average value of pressure across outlet; $p_{\text{average,inlet}} - p_{\text{average,outlet}}$	Output
$\Delta(\Delta T_{\text{cells}})$	Difference of the individual cell temperature gradients	Difference of the maximum individual cell temperature gradient (maximum$\{\Delta T_{\text{cell}}\}$) and the and minimum individual cell temperature gradient (minimum$\{\Delta T_{\text{cell}}\}$) in the module; $\Delta T_{\text{maximum, cell } x} - \Delta T_{\text{minimum, cell } y}$	Output
$T_{\max}$	Maximum temperature in module	Highest temperature in over all cells	Output

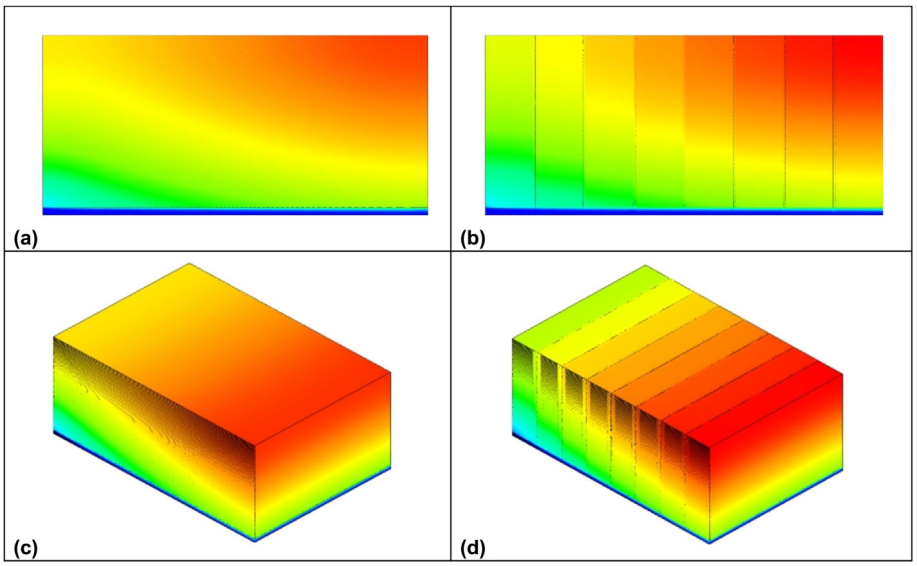

Fig. 5. Four considered models for an eight-cell battery module: (a) 2D block model, (b) 2D individual cell model, (c) 2D block model, and (d) 3D cell model.

compared to the three-dimensional models. Thus, the two-dimensional cell model describes the worse case in terms of thermal behavior.

3.3. The multi-objective analysis method and sample results

3.3.1. Method

Traditional one-dimensional total vehicle thermal management models assume a constant heat loss for various components along a coolant circuit. Consequently, the components are designed for a set coolant volumetric flow rate and inlet temperature. This single coolant operating point design method hinders the implementation of dynamic one-dimensional models that can drastically increase thermal management efficiency in the vehicle, which is especially important for range increases in electric- and hybrid electric vehicles. However, the increases in total system efficiency must not cause degradation to the individual components, making this method a valuable extension for finding the balance between the thermal behavior of the battery system and the total vehicle's thermal management system.

Using the two-dimensional ANSYS Fluent CFD-model described in the previous section in conjunction with Matlab, the thermal effect of various coolant operating conditions (coolant flow rate and inlet temperature) are calculated and displayed at various vehicle operating conditions. The steady state solution of the temperature gradient of each individual cell ($\Delta T_{\text{cell } n}$), the difference of the individual cell temperature gradients of the module ($\Delta(\Delta T_{\text{cells}})$), and the maximum module temperature ($T_{\max}$) are the quantities of interest for battery system thermal behavior. The pressure drop along the cooling plate (Δp) determines the coolant circuit pumping power (BTMS energy consumption), pump size, and pump cost. Complete definitions are shown in Table 2. Steady state solutions are used in the CFD-model in order to limit computational time (especially when coupled to a one-dimension model).

A higher $\Delta(\Delta T_{\text{cells}})$ indicates more diverse rates of aging of individual cells within a module, meaning that the decreased performance of a single cell could prematurely degrade total battery system performance. $T_{\max}$ is a further indication of cell aging, as temperatures above 35 °C decrease cell lifetime. Additionally, temperatures above 60 °C must be avoided (per the cell manufacturer's specifications) to reduce the risk of thermal runaway.

The interplay of the aforementioned quantities of interest are visually displayed by first making the quantities dimensionless—thereby allowing them to be simultaneously visualized—and second by plotting the dimensionless quantities versus coolant inlet temperature and volumetric flow rate. This allows a designer to optimize the vehicle thermal management system by selecting the ideal operating conditions and provides a dynamic input to the one-dimensional model. Furthermore, the data is plotted as a function of cell heat loss, reflecting various vehicle operating conditions.

3.3.2. Sample results

The multi-objective analysis method presented in Section 3.3.1 is demonstrated on the cooling plate geometry shown in Fig. 6 with a 0.5 mm top plate and 4 mm high fluid channel. Dimensionless data points are defined by dividing each data set by the maximum value in the set, allowing separate quantities such as $\Delta(\Delta T_{\text{cells}})$, $T_{\max}$ and Δp to be plotted on the same axis. Polynomial best fit surfaces are generated for the temperature data to eliminate peaks caused by the residuals from the applied convergence criteria in the CFD calculations. The best fit is achieved with a second order polynomial for the flow rate and a first order polynomial for the inlet temperature. The residuals from the best fit plots are in general highest at low volumetric flow rates, but R-Squared values of greater 0.97 are achieved.

The 3D-surface plots combined with the 2D-contour plots in Fig. 8 exhibit the effects of fluid flow rate and inlet temperature on

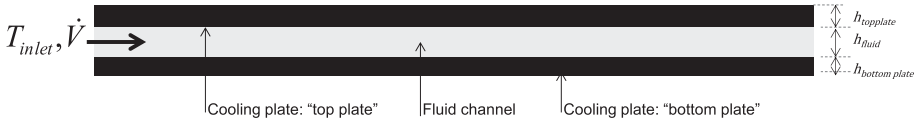

Fig. 6. Conceptual two-dimensional layout of a cooling plate.

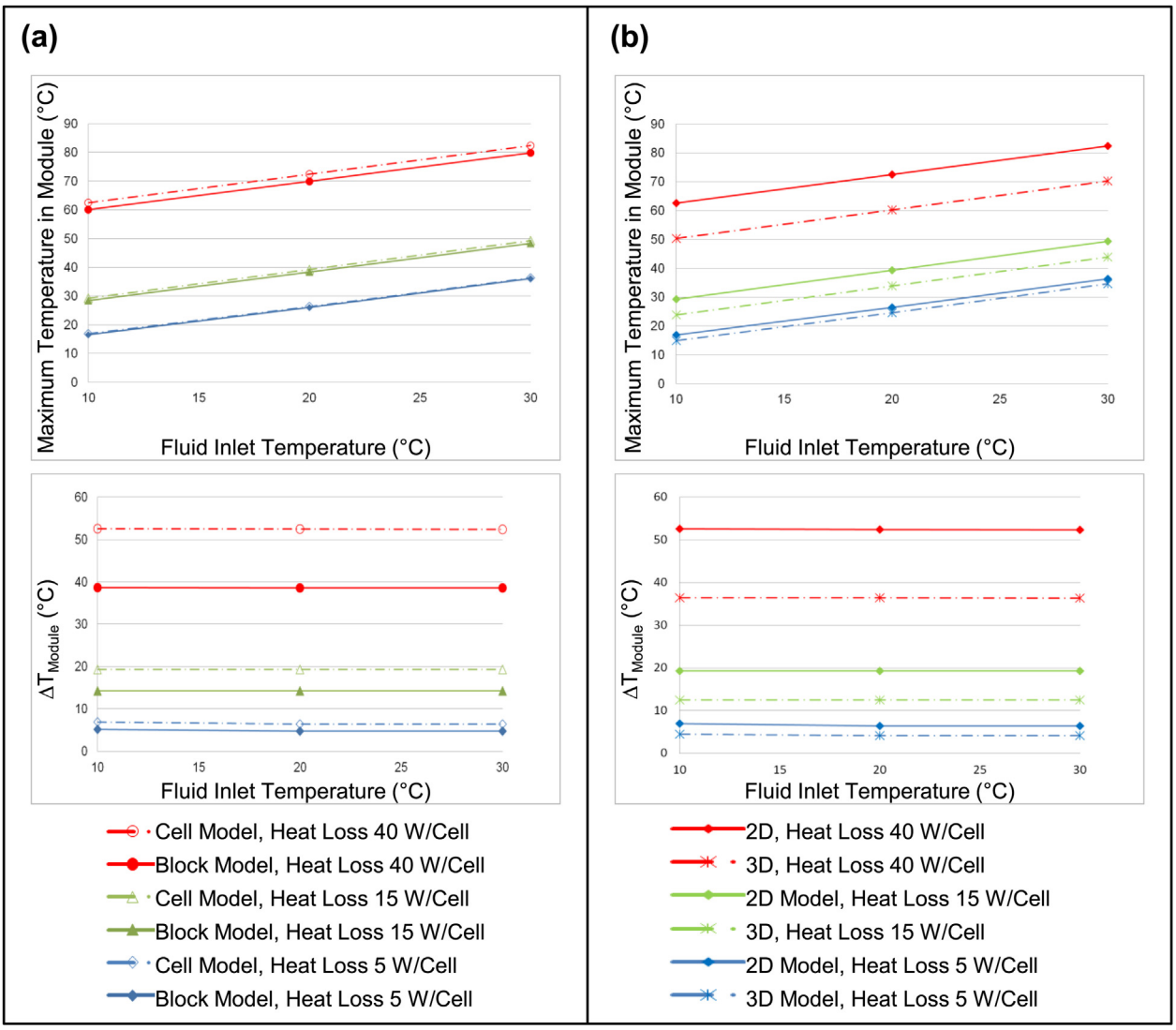

Fig. 7. Comparison of temperature difference and maximum temperature in module for (a) the cell and block models and (b) the two- and three-dimensional cell models.

both $\Delta(\Delta T_{cells})$ and T_{max}, showing the interplay between the quantities of interest.

Clearly, optimizing only for $\Delta(\Delta T_{cells})$, T_{max} or Δp can cause undesirable and even hazardous operating conditions for the battery cells, as flow rate has a greater influence on $\Delta(\Delta T_{cells})$, while inlet temperature has the greatest influence on T_{max}.

The influence of fluid flow rate and inlet temperature on $\Delta(\Delta T_{cells})$ and T_{max} is more evident at higher cell heat loss values, where as the pressure difference (Δp) barely changes as a function of the cell heat loss. The increasing influence of cell heat loss and the corresponding intersections of the $\Delta(\Delta T_{cells})$ and T_{max} surfaces with the Δp best fit surface are shown in Fig. 9.

The temperature difference over an individual cell, ΔT_{cell}, decreases along the flow direction of the cooling plate at low volumetric flow rates as shown in Fig. 10. Inlet temperature—just as over the entire module ($\Delta(\Delta T_{cells})$)—does not have an effect on ΔT_{cell} along the cooling plate.

Ultimately, the competing effect of coolant inlet temperature and flow rate on the maximum cell temperature, difference in the individual cell temperature gradients and the coolant pressure drop along the plate can be visualized using the presented analysis method, thereby allowing the thermal system designer to maximize the lifetime and capacity of the battery cells, and ultimately increase vehicle range. In the example presented, for example, a the designer can visualize the decreasing benefit of coolant flow rates above 20 L min^{-1} on $\Delta(\Delta T_{cells})$ as opposed to the increasing pressure drop.

4. Discussion

The presented method is universally designed, so that it can be implemented on any desired BTMS shape, or even any component requiring thermal management. Within the confines of an electric- or hybrid-electric vehicle, this analysis method can be performed on various components along the coolant circuit, and the resulting calculations can be stored and referenced by a one-dimensional model, helping optimize the efficiency of the total thermal management system.

The presented analysis method provides a means to optimize the performance of a BTMS for multiple competing objectives. As such, the effect of a wide range of input parameters from a vehicle's coolant circuit on the thermal behavior of the cells can be determined. The interplay and feedback from the one-dimensional coolant circuit models and three-dimensional BTMS models to

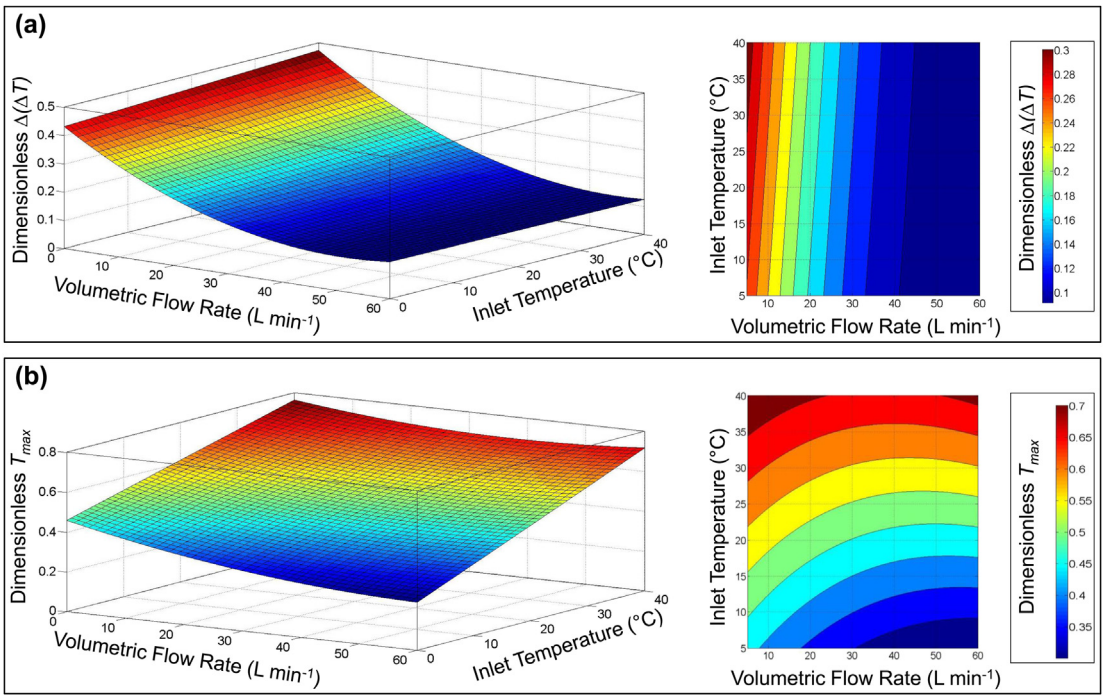

Fig. 8. Comparison of (a) temperature difference $\Delta(\Delta T_{cells})$ and (b) maximum temperature T_{max} in module as a function of fluid flow rate and inlet temperature for a cell heat loss value of 15 W/cell, each shown on surface and contour plots.

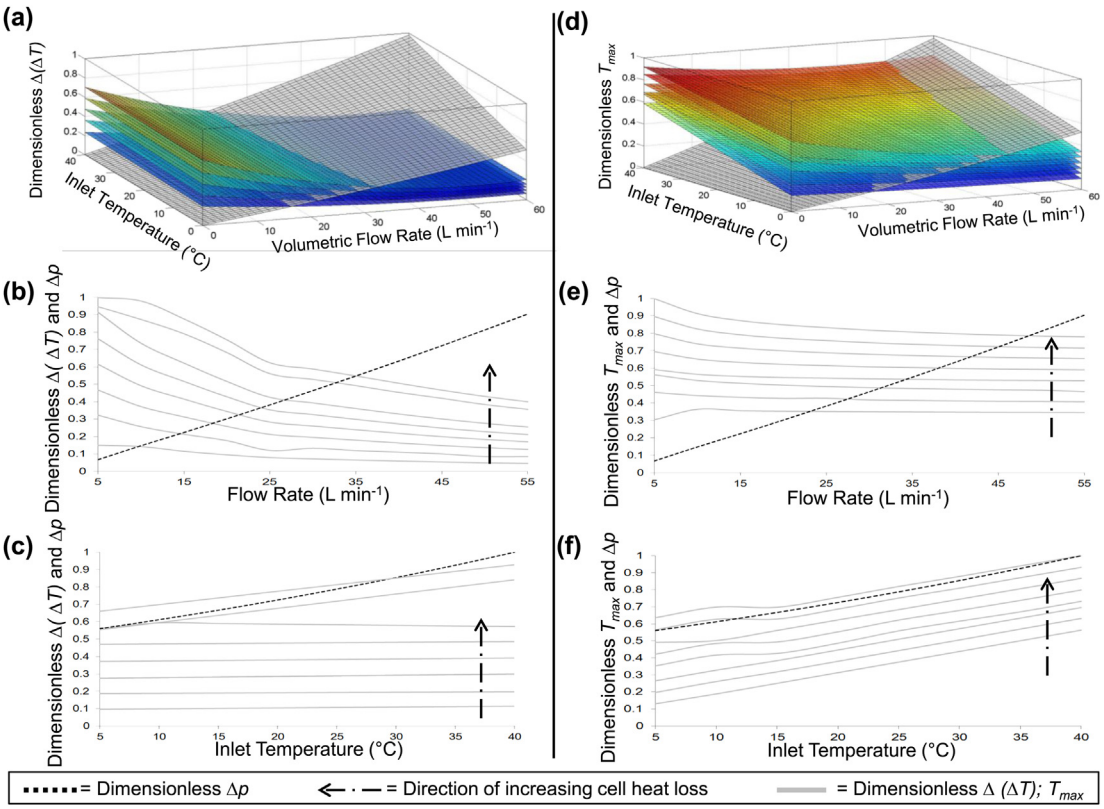

Fig. 9. Intersection of dimensionless best-fit plots of temperature difference $\Delta(\Delta T_{cells})$ with Δp (a) and maximum temperature T_{max} with Δp (d) in a module as a function of fluid flow rate and inlet temperature for various values of cell heat loss from 5 to 40 W/cell. Additionally shown are best-fit plots of temperature difference $\Delta(\Delta T_{cells})$ with Δp as a function of flow rate (b) and inlet temperature (c) and best-fit plots of maximum temperature T_{max} with Δp as a function of flow rate (e) and inlet temperature (f).

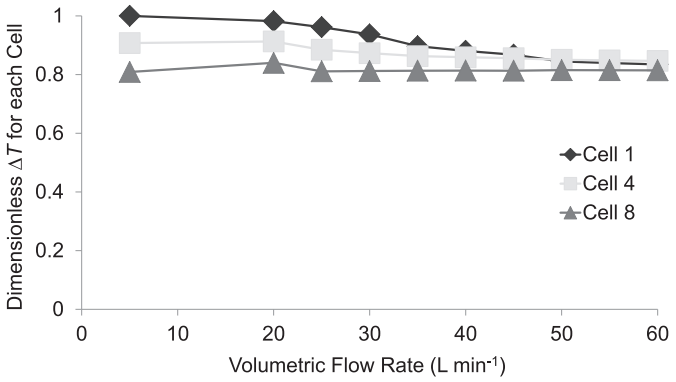

Fig. 10. Individual cell temperature gradients of the first, fourth and eighth cells (Cell 1, Cell 4 and Cell 8; along the flow direction) as a function of coolant flow rate at an inlet temperature of 10 °C and a cell heat loss of 15 W/Cell.

one another provide an efficient way to dynamically model the coolant circuit and determine total system efficiency. As such, conclusions can be drawn regarding whether, for example, electric vehicle range could actually be extended in the winter by drawing more power for the thermal management system, thereby increasing cell temperature and concurrently raising cell efficiency.

This analysis was performed on all possible combinations of coolant flow rate, inlet temperature, and cell heat loss: upon further implementation of this method a design of experiments to minimize the analyzed points, or a direct coupling with a one-dimensional model are recommended.

5. Conclusions

Using the analysis method, conclusions can be gathered about the optimal cooling plate operating conditions (coolant flow rate and inlet temperature) to guarantee ideal thermal conditions for the battery cells and reduce the energy consumption of the thermal management system (pressure drop). The results shown are merely a short application of the analysis method presented in this paper. This method can be applied to any thermal management system where a multi-objective optimization of competing criteria is required. Multi-objective optimization in general offers promise for the design of thermal management systems and will certainly play an increasing role in their development.

Acknowledgments

This research is funded by the research project *eProduction*, funded by the German Federal Ministry of Education and Research (BMBF), the project is part of the program STROM (Schlüsseltechnologien für die Elektromobilität, 13N12027). The authors thankfully acknowledge its financial support.

References

[1] Z. Rao, S. Wang, Renew. Sustain. Energy Rev. 15 (2011) 4554–4571.
[2] K. Smith, M. Earlywine, E. Wood, J. Neubauer, A.A. Pesaran, in: Proceedings of the 2012 SAE World Congress and Exhibition, Detroit, Michigan, April 24–26, 2012.
[3] T.M. Bandhauer, S. Garimella, T.F. Fuller, J. Electrochem. Soc. 158 (2011) R1–R25.
[4] A.A. Pesaran, M. Keyser, K. Smith, G.H. Kim, S. Santhanagopalan, in: Large Lithium Ion Battery Technology & Application Symposia Advanced Automotive Battery Conference, Pasadena, California, 2013.
[5] A. Pesaran, G.-H. Kim, in: 22nd International Battery, Hybrid and Fuel Cell Electric Vehicle Conference and Exhibition (EVS-22), Yokohama, Japan, 2006.
[6] T. Heckenberger, T. Himmer, F. Moldovan, M. Moser, R. Riedel, T. Schiehlen, M. Steinbach, Elektronikkühler und Verfahren zum Herstellen eines Elektronikkühlers, European Patent EP2575418A1, Issued April 3, 2013.
[7] C. Zahn, Thermally Conductive Plate Having a Network of Flow Channels, Method for Transport of Heat and Electrochemical Energy Storage, U.S. Patent US20130196207A1, Issued August 1, 2013.
[8] G. Katayama, K. Yamamoto, Battery Cooling Structure, U.S. Patent US20130146249A1, Issued June 13, 2013.
[9] S. Töpfer, Flüssigkeitswärmetauscher aus Kunstoff für ein Batteriekühlsystem, German Patent DE102013200859A1, Issued August 1, 2013.
[10] S. Weileder, S. Köster, R. Löffler, R. Lustig, A. Meijering, Device for Supplying Power, Having a Cooling Assembly, Patent WO2012013315A1, Issued February 2, 2012.
[11] A. Jarrett, I.Y. Kim, J. Power Sources 196 (2011) 10359–10368.
[12] H. Teng, Y. Ma, K. Yeow, M. Thelliez, SAE Int. J. Passenger Cars (2011) 1331–1342.
[13] P.A. Schmidt, T. Pauleser, M.F. Zaeh, in: Proceedings from Smart EV and HEV Battery Production, Darmstadt, Germany, April 22, 2013.
[14] S. Hirsch, C. Schmid, A. Wiebelt, M. Stripf, Thermisch Übergangsvorrichtung, Temperierplatte und Energiespeichereinheit, German Patent DE102011084002A1, Issued April 4, 2013.
[15] N. Daubitzer, M. Engelhart, T. Heckenberger, T. Himmer, Device for Pressing a Cooler Against a Battery, Patent WO2012/104394A1, Issued August 9, 2012, 2012.
[16] S.A. Syed, R.J. Heydal, J.G. Dorrough, Wave Fin Battery Module, U.S. Patent US20130101881A1, Issued April 25, 2013.
[17] T. Isermeyer, H. Damsohn, C. Pfender, Elektrochemische Energiespeichereinheit mit Kühlvorrichtung, European Patent EP2153487B1, Issued February 17, 2010.
[18] A. Schweizer, Formelsammlung – Berechnungsprogramme für Anlagenbau und Stromaggregate, Available at: http://www.schweizer-fn.de/stoff/kuehlwasser/kuehlw_start.php (accessed November 2013).
[19] R. Schwarze, CFD-Modellierung: Grundlagen und Anwendungen bei Strömungsprozessen, Springer Verlag, 2013, ISBN 978-3-642-24378-3.